PNAS Nexus, 2023, 2, 1–10
https://doi.org/10.1093/pnasnexus/pgad203
Advance access publication 21 June 2023
Research Report

Identification of small-molecule inhibitors against the interaction of RNA-binding protein PSF and its target RNA for cancer treatment

Ken-ichi Takayama[a], Seiji Matsuoka[b], Shungo Adachi[c], Teruki Honma[d], Masahito Yoshida[e], Takayuki Doi[e], Kazuo Shin-ya[c], Minoru Yoshida[f], Hiroyuki Osada[g] and Satoshi Inoue[a,h,*]

[a]Department of Systems Aging Science and Medicine, Tokyo Metropolitan Institute for Geriatrics and Gerontology, itabashi-ku, Tokyo 173-0015, Japan
[b]Seed Compounds Exploratory Unit for Drug Discovery Platform, RIKEN Center for Sustainable Resource Science, Wako, Saitama 351-0198, Japan
[c]National Institute of Advanced Industrial Science and Technology (AIST), Koto-ku, Tokyo 135-0064, Japan
[d]Drug Discovery Computational Chemistry Platform Unit, RIKEN Center for Biosystems Dynamics Research, Yokohama, Kanagawa 230-0045, Japan
[e]Graduate School of Pharmaceutical Sciences, Tohoku University, Sendai, Miyagi 980-8578, Japan
[f]Chemical Genomics Research Group, RIKEN Center for Sustainable Resource Science, Wako, Saitama 351-0198, Japan
[g]Drug Discovery Chemical Bank Unit, RIKEN Center for Sustainable Resource Science, Wako, Saitama 351-0198, Japan
[h]Division of Systems Medicine and Gene Therapy, Saitama Medical University, Hidaka, Saitama 350-1298, Japan
*To whom correspondence should be addressed: Email: sinoue@tmig.or.jp
Edited By: J. Silvio Gutkind

Abstract

Diverse cellular activities are modulated through a variety of RNAs, including long noncoding RNAs (lncRNAs), by binding to certain proteins. The inhibition of oncogenic proteins or RNAs is expected to suppress cancer cell proliferation. We have previously demonstrated that PSF interaction with its target RNAs, such as androgen-induced lncRNA *CTBP1-AS*, is critical for hormone therapy resistance in prostate and breast cancers. However, the action of protein–RNA interactions remains almost undruggable to date. High-throughput screening (HTS) has facilitated the discovery of drugs for protein–protein interactions. In the present study, we developed an in vitro alpha assay using Flag peptide–conjugated lncRNA, *CTBP1-AS*, and PSF. We then constructed an effective HTS screening system to explore small compounds that inhibit PSF–RNA interactions. Thirty-six compounds were identified and dose-dependently inhibited PSF–RNA interaction in vitro. Moreover, chemical optimization of these lead compounds and evaluation of cancer cell proliferation revealed two promising compounds, N-3 and C-65. These compounds induced apoptosis and inhibited cell growth in prostate and breast cancer cells. By inhibiting PSF–RNA interaction, N-3 and C-65 up-regulated signals that are repressed by PSF, such as the cell cycle signals by p53 and p27. Furthermore, using a mouse xenograft model for hormone therapy–resistant prostate cancer, we revealed that N-3 and C-65 can significantly suppress tumor growth and downstream target gene expression, such as the androgen receptor (AR). Thus, our findings highlight a therapeutic strategy through the development of inhibitors for RNA-binding events in advanced cancers.

Keywords: RNA-binding protein, alpha assay, high-throughput screening, hormone therapy–refractory cancer

Significance Statement

Hormone therapy–refractory cancer, such as prostate cancer and breast cancer, is one of the major clinical challenges worldwide. PSF, an RNA-binding protein (RBP), is overexpressed and promotes drug resistance in many cancers by modulating RNA-dependent signaling. However, targeting the action of RBPs for RNA modification for cancer treatment remains difficult. In the present study, we developed a cell-free strategy to identify small compounds that target the interaction of PSF with its target RNAs. We then identified potent inhibitors of PSF–RNA interactions using a high-throughput screening and subsequent chemical optimization. This study demonstrates that the small compounds can inhibit hormone therapy–refractory tumor growth, suggesting their efficacy in the treatment of advanced cancers.

Introduction

RNA-binding proteins (RBPs) have been implicated in the regulation of gene expression. RBPs are responsible for the maturation of target RNA through the formation of ribonucleoprotein complexes (1). Many RBPs play critical roles in numerous gene expression processes, including regulation of alternative splicing. Notably, dysregulated RBP function is important for the development of genetic and somatic diseases such as neurodegeneration,

Competing Interest: The authors declare no conflict of interest to disclose.
Received: May 25, 2023. **Accepted:** June 12, 2023

autoimmunity, and cancer (2, 3). A representative RBP, polypyrimidine tract–binding protein (PTB)–associated splicing factor (PSF) or splicing factor, proline, and glutamine-rich (SFPQ), participates in many aspects of RNA biogenesis, including transcriptional activation/repression and splicing (4–6). It is physiologically essential for neuronal differentiation and development (7–10). The resolved structures of PSF revealed a highly conserved DNA-binding domain (DBD), tandem RNA recognition motifs (RRMs), a nonA/paraspeckle domain (NOPS), and a C-terminal coiled-coil domain (6). In addition, a nuclear localization signal at the C-terminus promotes PSF distribution, predominantly in the nucleus close to chromatin or DNA damage loci (6). Thus, PSF is involved in both transcription and RNA processing (10–13). Importantly, recent studies have shown that changes in alternative splicing patterns by PSF are associated with tumorigenesis and therapeutic resistance (13–15).

PSF epigenetically suppresses target gene transcription by recruiting histone deacetylase (HDAC) enzymes to specific genomic binding regions (11, 12). In advanced prostate cancer, hormone therapy by androgen blockade significantly prolongs patient survival (16, 17). The main cause of hormone-refractory prostate cancer, termed castration-resistant prostate cancer (CRPC), is the amplified signals of the androgen receptor (AR) (18). Therefore, the mechanisms underlying enhanced AR downstream signaling could be promising drug targets for hormone-refractory prostate cancer. We have previously reported that *CTBP1-AS*, an androgen-induced lncRNA in the antisense region of carboxyl-terminal binding protein 1 (CTBP1), promotes castration-resistant prostate tumor growth (11). *CTBP1-AS* modulates global epigenetic status by interacting with PSF and its associated HDAC complex to repress cell cycle regulators or CTBP1 (AR corepressor) for tumor growth and activate AR activity. We also showed that PSF binds to pre-mRNAs and coordinate the expression and complex formation of various spliceosome factors at the RNA level in advanced prostate cancer (13). Dysregulation of the spliceosome complex enhances the spliceosome activity of AR and the production of its variant through RNA-level regulation. Moreover, aggressive types of tumors in breast cancer, which develop due to excessive estrogen receptor α (ERα)–mediated signals, show resistance to hormone therapy using an ERα antagonist, such as tamoxifen (19–22). In ERα-positive breast cancer, PSF binds to the pre-mRNAs of tumor-promoting genes, such as *ERα* (*ESR1*) and *Sec1 family domain containing 2* (*SCFD2*), to regulate the mRNA level at the posttranscriptional level (23). Thus, PSF confers resistance to 4-hydroxytamoxifen (OHT) in breast cancer tumor growth. Therefore, we specifically aimed to identify bioavailable small molecules targeting PSF, with preferential cytotoxicity in hormone-refractory prostate and breast cancer cells. By investigating PSF-associating molecules using high-throughput screening (HTS) of small-molecule libraries using chemical arrays, we previously identified a compound, No. 10-3 (7,8-dihydroxy-4-(4-methoxyphenyl)chromen-2-one), that disrupted PSF complex formation, PSF-mediated RNA splicing, and the epigenetic pathway (24). Treatment with No. 10-3 promotes apoptosis and impairs the cell cycle in both breast and prostate cancer cells.

Interaction of RNAs, including lncRNA or pre-mRNA, with RBPs is a key determinant for directing RNA functions and maturation (25, 26). However, the activity of RNA or its interaction with RBP mainly remains "undruggable" due to the challenging identification of small molecules that modulate this process. Protein–protein interactions (PPI) are important for all cellular processes and functions because proteins form specific noncovalent complexes with other cellular proteins (27–29). PPI regulator screening is a method in discovering drug candidates using modern proteome analyses, such as Förster resonance energy transfer (FRET) and alpha assays (30–32). The fluorescence emitted by the interaction is measured in these analyses. However, the absence of a unitary and readily measurable system to detect the physical interaction of RNA–protein interactions (33, 34) makes screening of compounds difficult. In the present study, we aimed to develop an assay capable of screening a large number of compounds that directly target the interaction of PSF with RNA. We constructed an in vitro alpha assay using synthesized Flag peptide–conjugated RNA molecules to detect such interactions. This assay was then used to screen a collection of pharmacologically active compounds, with rapid confirmation of binding. In accordance with the binding data and medical chemistry optimization, two molecules (N-3 and C-65) demonstrated dose-dependent inhibition of PSF–RNA interaction. Notably, the pharmacological inhibition of PSF by these compounds suppressed tumor growth in vivo without obvious adverse effects. Thus, our findings highlight PSF–RNA interactions as promising target events for treatment-resistant cancer. Of note, our results show the possibility that this approach would be useful for identifying active drug candidates that target lncRNA function by binding to RBPs.

Results

Construction of in vitro cell-free system to detect RBP–RNA interaction using alpha assay technique

First, we aimed to develop a cell-free assay method for the high-throughput detection of small molecules by combining RNA alkylation with the alpha assay technique. To detect the interaction of PSF with *CTBP1-AS*, we conjugated *CTBP1-AS* RNA probes with a Flag peptide (Supplementary Fig. S1A) via alkylation to obtain FLAG-tagged RNA probes (Supplementary Fig. S1B). Alkylation was confirmed by conjugating the Flag peptide to the short RNA. A mobility shift was observed using gel shift assay to demonstrate the successful RNA–protein conjugation reaction (Fig. 1A). Subsequently, we conjugated *CTBP1-AS* probes produced by in vitro transcription with Flag peptide via alkylation. To confirm alkylation, immunoprecipitation of *CTBP1-AS* probes with or without Flag conjugation added to 22Rv1 nuclear lysate was performed using anti-Flag antibodies and qRT-PCR analysis revealed the efficient enrichment of *CTBP1-AS* tagged with FLAG (Fig. 1B). The in vitro pull-down assay demonstrated the interaction of Flag-tagged *CTBP1-AS* with endogenous PSF protein in 22Rv1 nuclear lysate (Supplementary Fig. S1C) and His-tagged PSFΔC (His-ΔC-PSF) (1–460 aa) proteins produced in *Escherichia coli* (Fig. 1C), suggesting that the interaction is direct. Consistently, this interaction is diminished by RNase treatment or excessive competitors (unlabeled RNA), suggesting this interaction is dependent on Flag–*CTBP1-AS* (Supplementary Fig. S1C and D). Furthermore, we analyzed this interaction using the alpha assay technique (Fig. 1D). The alpha assay signal was generated when His-tagged ΔC-PSF–coated nickel acceptor beads were brought in close proximity to Flag-tagged *CTBP1-AS*-coated flag donor beads through binding between tagged RNA and RBP. We detected alpha assay signal by increasing the concentration of ΔC-PSF concentration (Fig. 1E). In addition, we observed that the alpha assay signal dose-dependently increased in parallel with *CTBP1-AS* concentration (0–0.63 nM) (Fig. 1E).

Selection of candidate PSF–RNA interaction inhibitors using in vitro alpha assay system

To identify compounds disrupting the interaction of PSF with its RNA targets, the alpha assay system was used as readout in a

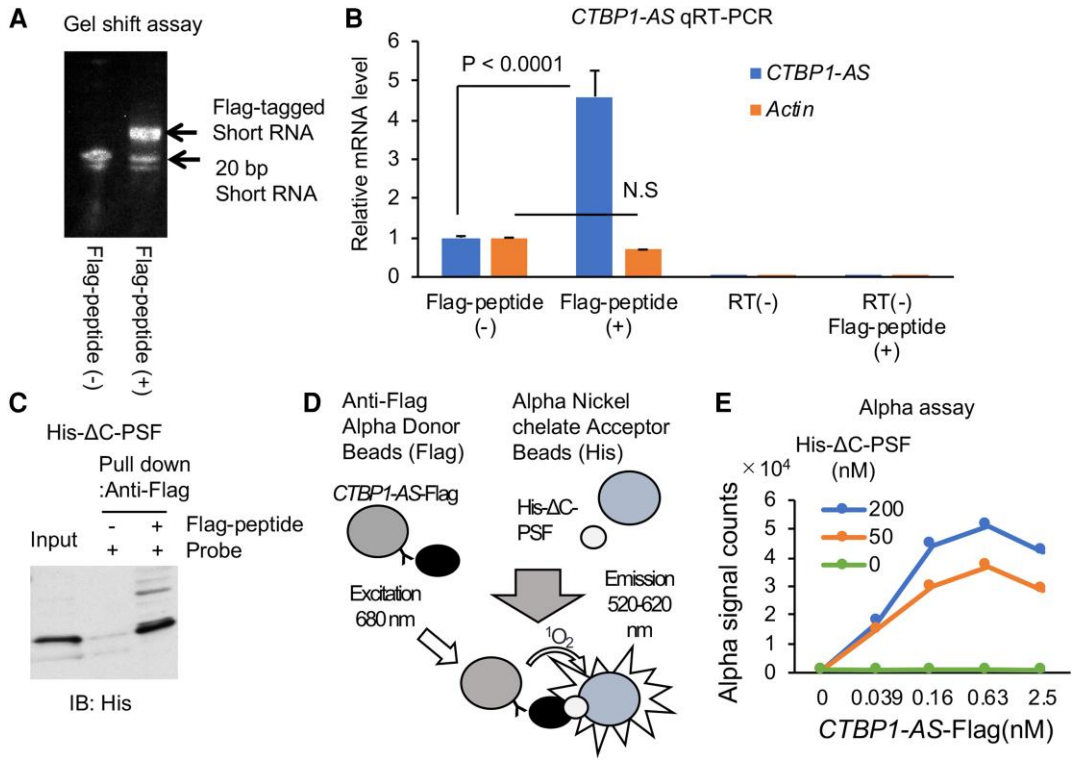

Fig. 1. Detection of PSF and RNA interaction by in vitro alpha assay system. A) Alkylation of RNA with Flag peptides. The gel shift assay indicated the conjugation of the Flag peptide with short RNA (miR-21: 20 bp). B) Immunoprecipitation of Flag–*CTBP1-AS*. *CTBP1-AS* probe with or without Flag modification was added to 22Rv1 nuclear lysates and then immunoprecipitated with an anti-Flag antibody. qRT-PCR analysis ($N = 3$, technical replicates) was performed to measure the *CTBP1-AS* RNA levels. RT, reverse transcriptase. β-Actin is used as a negative control gene. One-way ANOVA and Tukey's post hoc tests were performed to obtain *P*-values. Data are presented as the mean ± SD. C) In vitro RNA pull-down of His-ΔC-PSF produced in *E. coli* using a Flag–CTBP1-AS probe. D) Schematic representation of reconstituted PSF–RNA interactions. His-ΔC-PSF could bind to Flag–*CTBP1-AS*. The chemical energy of the reactive oxygen on the donor beads was transferred to the acceptor beads, and a signal was detected. E) Dose-dependent detection of PSF–RNA interaction by in vitro alpha assay system. Nickel acceptor beads and Flag donor beads were incubated with His-ΔC-PSF and Flag–*CTBP1-AS*. The mixture was then incubated for 20 min at room temperature before measuring the alpha signals ($N = 2$, biological duplicates; data are presented as the mean).

HTS of several chemical libraries (35–38), which include a total of 55,961 compounds. In these assays, we evaluated the effects of the compounds by measuring the signal in in vitro alpha assay (Fig. 2A). Compounds that inhibited the alpha signals (>30%) were considered as initial hits and suppressed the interaction between PSF and RNA (Fig. 2B).

Next, we performed a second screening to select active compounds that exhibited dose dependency and excluded compounds that were frequently observed in other screenings (Figs. 2C and S2). A total of 36 compounds that reduced alpha signals with reproducibility were defined as potential inhibitors of PSF–RNA interaction (Supplementary Fig. S2). None of the selected compounds showed false positive reactions (Supplementary Fig. S2), suggesting specific inhibition of PSF interaction.

Secondary screening and evaluation of active compounds in hormone therapy–refractory prostate cancer cells

Furthermore, we evaluated these 36 hit compounds through a second screening assay. An RNA pull-down assay was performed to assess the disruption of PSF–RNA interaction using nuclear lysates of prostate cancer 22Rv1 cells. We observed a reduction in the PSF–RNA interaction for all compounds at a concentration of 10 μM (Supplementary Fig. S3A). Furthermore, 11 compounds efficiently inhibited this interaction at a low concentration (1 μM) (Supplementary Fig. S3B). To test whether these compounds were active in cancer cells, we evaluated the effect on the inhibition of cell viability by inhibiting PSF–RNA interaction. We observed that six molecules (N-3, N-4, N-6, N-16, N-18, and K-9) inhibited cell viability, suggesting that they were active in cells (Figs. 3A and S4A). Interestingly, these molecules suppress cell growth in hormone therapy–resistant 22Rv1 cells at a lower concentration compared with that in sensitive LNCaP cells, consistent with our previous studies (13, 24), which showed an increased expression of PSF in hormone therapy–resistant cells (Figs. 3A and S4B).

Of the 11 candidates, 7 compounds (N-3, N-4, N-11, N-16, N-17, K-9, and S-1) with possible drug-like features (39–41) were selected for further analysis. We observed dose-dependent inhibition of PSF–RNA interactions using RNA pull-down assays (Figs. 3B and C and S5A). Thus, we determined the IC_{50} values (<1 μM) of these compounds (Supplementary Fig. S5B). Among them, highly efficient inhibition of PSF–RNA interaction was observed by the addition of N-11, N-17, and N-16.

Chemistry optimization revealed enhanced potency for inhibiting hormone-refractory cancer cell growth and apoptosis induction

Subsequently, we performed similarity searches of the seven hit compounds with determined IC_{50} values to enhance potency and analyze the structure–activity relationship (Supplementary Fig. S6A). To obtain compounds with more efficient antitumor

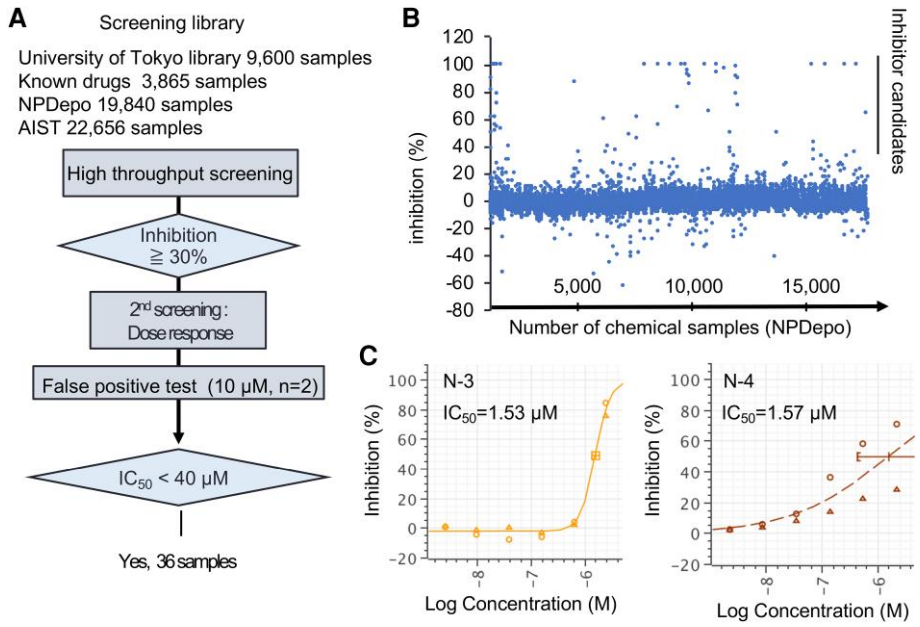

Fig. 2. HTS of chemical libraries using in in vitro alpha assay system detecting PSF–RNA interaction. A) The procedure for the PSF–RNA alpha screening technique was presented. We found 36 samples by primary HTS and a second screening by analyzing dose-dependent responses and false positive tests using biotin and streptavidin. B) Primary screening of core chemical libraries using in vitro PSF–RNA interaction system. The results presented are the result of the NPDepo library. C) Dose-dependent inhibition of PSF–RNA interaction. IC_{50} was calculated ($N = 2$, biological duplicates).

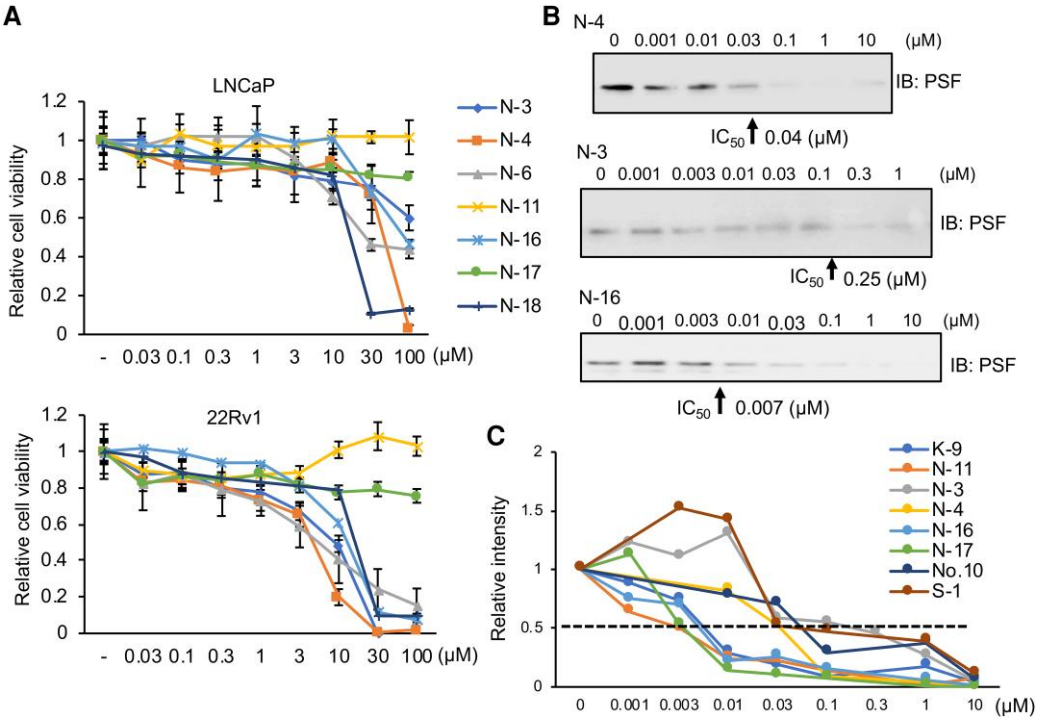

Fig. 3. Inhibition of cell growth of hormone therapy–resistant prostate cancer cells and PSF–RNA interaction by identified small compounds. A) Cell viability was determined by MTS assay in prostate cancer cells (22Rv1 and LNCaP cells) treated with each small compound ($N = 4$, biological replicates). Data are presented as the mean ± SD. B) Inhibition of the interaction between PSF and RNA in vitro. RNA pull-down assays were performed using 22Rv1 and biotin-labeled *CTBP1-AS* RNA probes. The cell lysates were mixed with each compound and used in the assay. IB, immunoblot. C) Determination of IC_{50} for RNA pull-down assay. Each band in the western blot analysis was quantified and plotted. No. 10 is a small molecule targeting PSF activity we found in the previous study (22).

activity, a total of 53 potential candidates were screened by analyzing their effects on cancer cell viability (Supplementary Fig. S6B). For this screening assay, we used the OHT-resistant OHTR cell line established from MCF7 cells (23) as a hormone-refractory breast cancer model, in addition to 22Rv1 cells. We discovered that C-65, which has a modified N-3 structure, could suppress the viability of both cell lines at a low dose (1 μM). Thus, we chose C-65 as the potent lead compound impairing PSF–RNA interaction

and compared its activity in vitro and in vivo with that of N-3 (Fig. 4A).

We assessed the effects of C-65 on the interaction between PSF and *CTBP1-AS* RNA probes. Surprisingly, RNA pull-down assay revealed that the IC_{50} of C-65 for inhibition (0.02 μM) was much lower than that of N-3 (0.25 μM), showing the enhanced molecular activity by optimization (Figs. 4B and S6C). We performed western blot analysis to examine the effects of N-3/C-65 on cell signaling pathways, such as p53, p21, and p27, which are epigenetically regulated by PSF (11, 13, 24) (Fig. 4C). We observed the induction of p53 and its target p21 in p53 wild-type cells (22Rv1 and OHTR cells), as well as p27 in both p53 wild type and p53 mutant cells (DU145 and MDA-MB-231 cells). However, the effect of C-65 addition on p27 induction was not as evident as that of N-3 in DU145 cells. We also observed apoptotic markers such as cleaved PARP1 and BAX were induced in both prostate and breast cancer cells.

Next, we tested the cytotoxic effects of N-3/C-65 on cancer cells. First, MTS assay was performed on both p53 wild-type and hormone receptor–positive cells (AR in prostate and ERα in breast cancer cells) (Fig. 4D). Consistent with the action of C-65 against PSF–RNA interaction, C-65 treatment blocked OHTR and 22Rv1 cell growth with an IC_{50} of 1 and 4 μM, respectively, more efficiently than N-3. Interestingly, these effects were not evident in hormone therapy–sensitive models MCF7 and LNCaP cells (Supplementary Fig. S7A). We next examined the effect of C-65 on p53 mutant type and hormone receptor–negative DU145 and MDA-MB-231 cells (Fig. 4D). In MDA-MB-231 cells, PSF expression level was lower than that in OHTR (Figs. 4C and S6D). The effects of N-3 and C-65 on cell growth were not evident compared with OHTR. However, a lower IC_{50} was observed in MDA-MB-231 cells treated with C-65 (20 μM) than in those treated with N-3. A similar effect was observed in DU145 cells. Notably, the inhibitory effects of these compounds on the growth of fibroblast cells (TIG3) and benign human prostate epithelial cells (RWPE) were not observed (Supplementary Fig. S7A). To show the effect of the small molecules (N-3 and C-65) is specific to PSF, we used LNCaP cells overexpressing PSF and control cells. We observed cell proliferation is more severely inhibited by C-65 and N-3 addition in PSF overexpressing cells compared with control, suggesting that the drug response is dependent on PSF (Fig. 4E). Furthermore, we evaluated the effects of these compounds on the induction of apoptosis. Consistent with the results of western blotting, these compounds significantly induced apoptosis in both prostate and breast cancer cells (Supplementary Fig. S7B). Thus, these results indicate improved activity by chemical optimization to repress cancer cell growth and induce apoptosis.

N-3 and C-65 significantly inhibit hormone-refractory prostate tumor growth and impair PSF-driven gene expression in vivo

We further investigated the potency of pharmacologically targeting PSF–RNA associations with N-3 and C-65 by using an in vivo xenograft model of AR-positive 22Rv1 cells. We performed castration to inhibit androgen action to mimic hormone therapy in mice. Castration-resistant tumor growth was markedly inhibited by these compounds (10 mg/kg, three times per week) (Fig. 5A and B). Meanwhile, significant toxic effects were not observed, such as body weight change (Fig. 5C). In surrounding tissues, we observed no obvious change to organs such as kidney. qRT-PCR analysis showed decreased mRNA expression levels of PSF-target RNAs in 22Rv1 cells, *AR*, and lncRNA *SchLAP-1* (13, 24) in tumors treated with C-65 (Fig. 5D). Moreover, western blotting showed dramatically repressed AR protein levels and p27 and p53 induction in tumors (Fig. 5E and F). Accordingly, we confirmed that apoptotic changes were enhanced by C-65 treatment in vivo compared with N-3 treatment by detecting PARP cleavage using western blot analysis. In addition, we observed that histone acetylation levels in tumors were increased compared with vehicle control samples, indicating the blockade of PSF-mediated histone deacetylation activity (Fig. 5F and G).

Moreover, the efficacy for hormone therapy–resistant cancer growth was examined by combining N-3 or C-65 with hormone therapy drugs. Whereas we observed that N-3 or C-65 inhibited cell viability of hormone therapy–resistant OHTR or 22Rv1 cells, treatment with hormone therapy drugs including OHT or enzalutamide (Enz) did not significantly. However, addition of N-3 or C-65 plus hormone therapy reagents further decreased cell viability, which indicates that hormone therapy sensitivity could be restored by combinational treatment (Supplementary Fig. S8).

Based on these data, we propose that the active compounds identified using our RBP–RNA assay screening system can potently inhibit the PSF-downstream signaling pathway and hormone therapy-refractory cancer growth.

Discussion

In this study, we aimed to develop a small-molecule PSF inhibitor that can block the formation of RBP complexes in the nucleus and is suitable for potential cancer treatment. Drugs for prostate cancer treatment, including Enz, inhibit androgen signaling, which is the major growth-promoting pathway mediated by AR, and are effective in repressing tumor growth. Despite these initial successful treatments, aggressive cancers that grow in castrate levels of androgen, termed CRPC, remain a significant clinical problem (16). Previous studies have identified the underlying mechanisms would be enhanced AR-driven gene regulation and amplified expression of AR and its splice variants lacking the ligand-binding domain (ARVs) in CRPC (42). We previously showed that high expression levels of PSF are supposed to promote the formation of splicing complexes for AR and its variant production in CRPC tissues (13). Furthermore, we have demonstrated that high PSF expression is associated with recurrence and poor survival in ER+ breast cancer, although selective estrogen receptor modulators, such as tamoxifen, are one of first-line treatments for ER+ breast cancer (23). We revealed that inhibition of PSF can overcome endocrine therapy resistance in ER+ breast cancer cells, suggesting the critical role of PSF in the progression of this disease (23). Consistently, other recent reports have also suggested that aberrant PSF expression is a major factor in the development of several treatment-resistant cancers (14, 15, 43–45). Therefore, we expect that this therapeutic approach targeting the interaction of PSF with RNAs will be useful for overcoming treatment resistance in such types of cancers.

As an important step in PSF function, RNA–protein interactions have been assumed to be undruggable although these act as an important working point. To solve this problem, we developed a promising screening strategy by applying an alpha assay system with chemically modified RNA via conjugation with tagged peptides. In the present study, we combined HTS (28) with a biomolecular method for detecting protein–RNA interactions using alkylation-mediated RNA modulation with Flag peptide in vitro. The technique developed by this study has two advantages. First, in combination with alpha assay screening, we could analyze a large number of small compounds using purified PSF

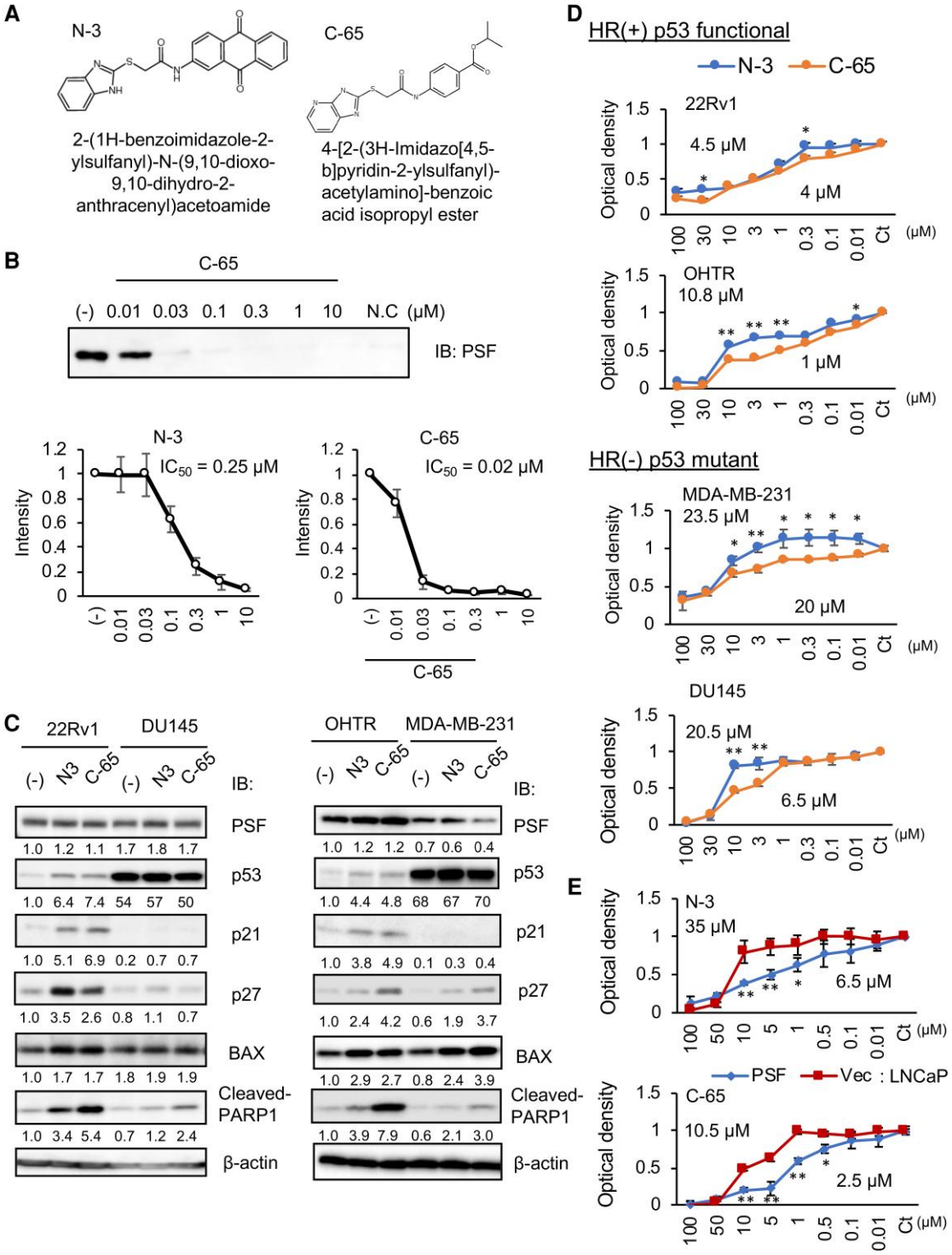

Fig. 4. Chemical optimization identified a molecule with increased antitumor efficacy in cells. A) Structure of N-3 and optimized C-65. B) Inhibition of the interaction between PSF and RNA in vitro by C-65. RNA pull-down assays were performed using 22Rv1 and biotin-labeled *CTBP1-AS* RNA probes. The cell lysate was mixed with C-65 and used in the assay. IB, immunoblot. Quantified protein expressions of PSF obtained by RNA pull-down ($N = 3$, biological replicates) are plotted. Effects of both N-3 and C-65 treatments were evaluated by estimating IC_{50}. Data are presented as the mean ± SD. C) The regulation of the cell cycle and apoptosis in prostate and breast cancer cells was analyzed by western blot analysis. Cells were treated with N-3 and C-65 (10 μM) or vehicle for 72 h. DU145 and MDA-MB-231 cells harboring p53 mutations. Quantified protein levels are shown as numbers. D) Cell viability was determined by MTS assay in prostate cancer cells treated with N-3 and C-65 ($N = 4$, biological replicates). The IC_{50} of N-3 and C-65 in repressing cell viability is shown on the left (N-3) or right (C-65). HR, hormone receptor; Ct, vehicle control. Two-sided *t* test was performed to determine the statistic difference between N-3 and C-65 treatments. $^*P < 0.05$ and $^{**}P < 0.01$. E) Cell viability was determined by MTS assay in LNCaP cells overexpressing PSF and vector control cells (Vec) treated with N-3 and C-65 ($N = 4$, biological replicates). The IC_{50} of N-3 and C-65 in repressing cell viability is shown on the left (Vec) or right (PSF). Ct, vehicle control. Two-sided *t* test was performed to determine the statistic difference between PSF and vector control cells. $^*P < 0.05$ and $^{**}P < 0.01$. Data are presented as the mean ± SD.

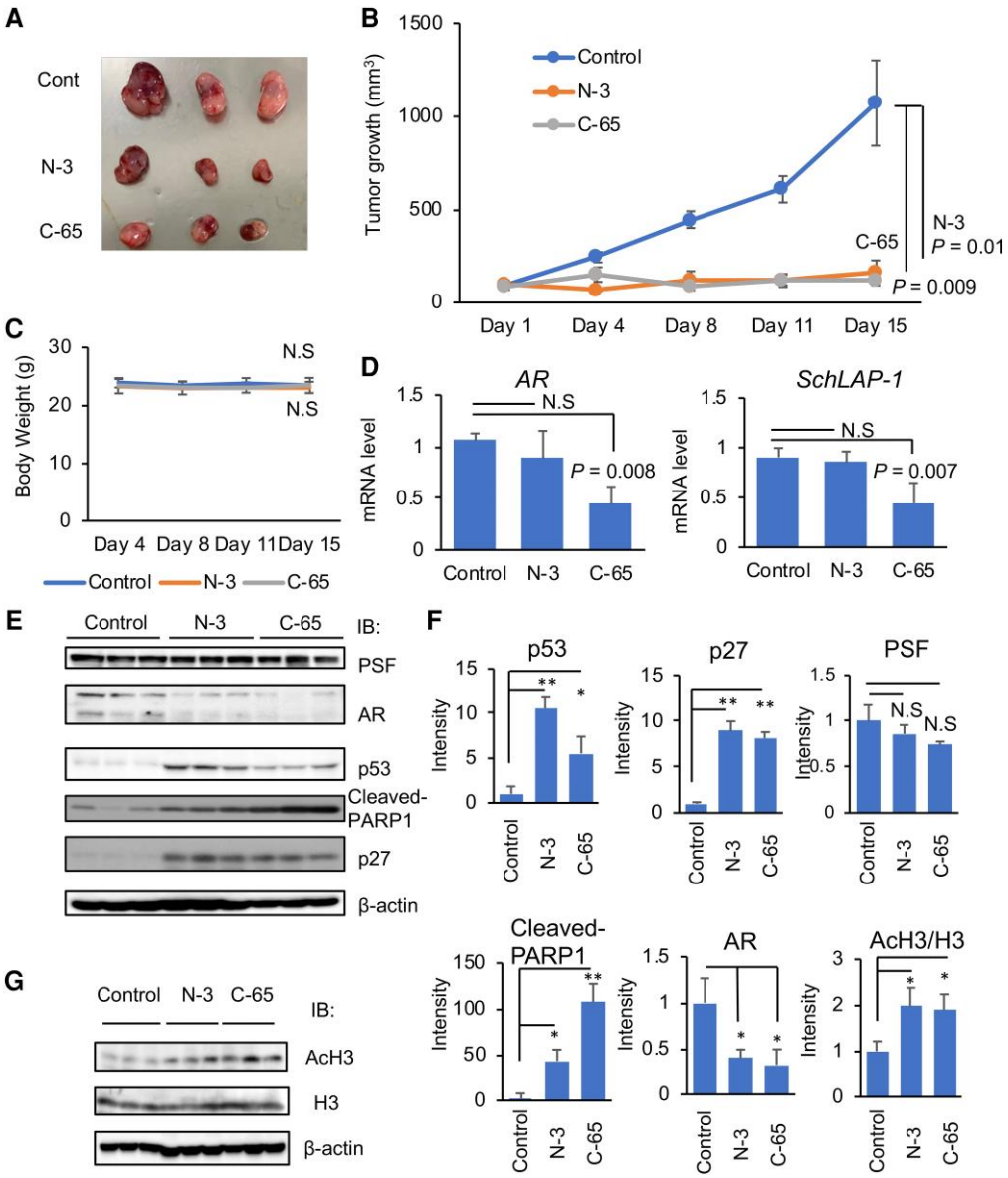

Fig. 5. Therapeutic efficacy of N-3 and C-65 in xenograft model of hormone therapy–resistant prostate cancer. A) 22Rv1 cells were inoculated subcutaneously into nude mice. After tumor development, mice were castrated. The treatment group was administered N-3 or C-65 (10 mg/kg) three times per week ($N = 6$, biological replicates). The control group was treated with the vehicle. Representative images of tumors treated with control, C-65, and N-3. The tumor volume B) and body weight C) were measured twice per week. Statistical difference was determined by one-way ANOVA and Tukey's post hoc tests. Data are presented as the mean ± SD. D) mRNA levels of PSF target genes at the RNA level were determined by qRT-PCR ($N = 4$, biological replicates). Total RNA was extracted from the tumors treated with the indicated compounds. One-way ANOVA and Tukey's post hoc tests were performed to obtain *P*-values. Data are presented as the mean ± SD. E) N-3 and C-65 down-regulated PSF target signals and activated apoptosis signaling. Lysates from multiple tumor tissues ($N = 3$, biological replicates) were used for western blot analysis to detect the indicated protein levels. IB, immunoblot. F) Quantification of protein expressions in tumors ($N = 3$, biological replicates). β-Actin and H3 are used as a loading control for normalization of protein expressions. One-way ANOVA and Tukey's post hoc tests were performed to obtain *P*-values. $^{*}P < 0.05$ and $^{**}P < 0.01$. Data are presented as the mean ± SD. G) Western blot analysis of activated histone acetylation after N-3 and C-65 treatment of tumors.

proteins and Flag-tagged RNA by performing multianalyte evaluation and automated analysis of compounds. Second, a cell-free assay approach to find hits was conducted to include the compounds that target the interaction between RNA and PSF but lack the molecular property to cross cell membranes, which could be potential lead compounds. Then, we successfully showed dose-dependent disruption of PSF–RNA interaction using the identified small compounds.

It is important to analyze whether these small molecules act on the PSF or RNA as molecular mechanism for this inhibition. Although we investigated PSF-binding molecules in the previous study (24), we did not identify these small molecules obtained in this alpha screening assay as PSF-binding molecules. In addition, PSF protein lacking C-terminal domain (deleted protein more specific for RNA binding) is used for this alpha screening. The conformational change in the RNA-binding domain may be caused by RNA binding. We speculate these conformations by PSF and RNA are targeted by these small molecules. In vitro assay to investigate the interaction between small molecules and PSF or RNA would be important to further determine how these molecules

act to inhibit the interaction. Further insights into the cellular function of PSF induced by these small compounds could aid in understanding the pathogenesis of advanced cancer.

Notably, N-3 and C-65 treatment induced cell apoptosis and inhibited cancer cell growth. Interestingly, this effect was more evident in hormone therapy–resistant model cells (OHTR and 22Rv1) than in sensitive cells (LNCaP and MCF7) or human nonmalignant cells. These observations may reflect the high expression levels of PSF in these hormone therapy–resistant model cells. Furthermore, we demonstrated that N-3 and C-65 could significantly inhibit PSF-target gene expression in a hormone-refractory prostate cancer in vivo model. AR is an important target of PSF at the RNA level (13). Namely, pre-mRNA binding of PSF to AR enhanced AR expression. Furthermore, we revealed that C-65 treatment reduced the AR expression at both the mRNA and protein levels in vivo more efficiently than N-3, consistent with the more robust inhibition of PSF–RNA interaction with C-65 compared with N-3. Moreover, we have demonstrated that cell cycle regulators p53 and p27 are regulated by PSF via epigenetic mechanisms (11, 13, 24). In an androgen-dependent mechanism, the *CTBP1-AS* and PSF complex is recruited to the promoter of p53 to repress its expression. We observed the up-regulation of p53 signaling in wild-type p53 cancer cells (22Rv1 and OHTR) following treatment with C-65 and N-3. Importantly, these treatments induced p27 in cancer cells harboring p53 mutant, suggesting that alternative PSF-driven gene regulations including p27 participate in p53 mutant cancer cells. Meanwhile, we could not detect significant differences in the ability of N-3 and C-65 to repress tumor growth and induce p53 and p27 in tumors. It is tempting to speculate that other effects of these compounds on PSF proteins such as epigenetic controls at gene promoters independent of RNA-binding events (23) might be involved in these results. Moreover, the effects of C-65 treatment were evident in breast cancer cells. We can assume cancer-type specific effects of these compounds in repressing PSF signals.

Overall, our study aids in the development of drugs that target oncogenic transcriptional and splicing modifiers. We provide a feasible strategy for identifying compounds that target the working points of RBPs associated with RNAs including lncRNAs. Considering that PSF is also an important oncogenic gene in several other types of cancer, future studies will be required to evaluate whether C-65, N-3, and No. 10-3 could be effective in other cancers. Importantly, RBP–RNA interaction is associated with a wide variety of human diseases. The present screening strategy can contribute in the development of useful drugs that target RNA modifications to improve human health.

Materials and methods

Conjugation of Flag peptide to *CTBP1-AS* RNA probe

Sodium periodate ($NaIO_4$), sodium cyanoborohydride ($NaCNBH_3$), and lithium perchlorate ($LiClO_4$) were purchased from Sigma-Aldrich. Alkylation was performed as previously described with some modifications (46, 47). Briefly, freshly prepared 0.5 mL of 0.1 M $NaIO_4$ was added to 10 μM *CTBP1-AS* RNA probe produced via in vitro transcription, and the mixture was incubated at 0°C for 20 min. The 3′-dialdehyde RNA was precipitated with 14 mL of 2% $LiClO_4$ in acetone and then washed with 1 mL acetone. The pellet was dissolved in 5 μL of 0.1 M sodium acetate (pH 5.0) and then mixed with 0.25 mg Flag peptide. The reaction solution was mixed at room temperature for 3 h. The resulting imine moiety of the RNA–Flag was reduced by adding 10 μL of 1 M $NaCNBH_3$ and then incubated at room temperature for 30 min. We obtained purified Flag-conjugated RNA using an RNA purification column (Qiagen, Hilden, Germany). The alkylation efficiency was estimated by measuring the amount of Flag–RNA recovered using NanoDrop. We used miRNA (miR-21; Thermo Fisher) to confirm the conjugation between RNA and Flag peptide using a gel shift assay. After the reaction, the reaction products were analyzed using denaturing urea polyacrylamide gel electrophoresis (15% acrylamide gel) with ethidium bromide staining.

Alpha assay screening

Flag–*CTBP1-AS* (0.63 nM) was prepared with anti-FLAG alpha donor beads (20 μg/mL) and 0.5 mM dithiothreitol (DTT) in assay buffer [25 mM Tris–HCl (pH 7.5)], 150 mM potassium chloride, and 0.5% NP-40 for 3 h at 4°C. The 50-nM His-ΔC-PSF protein was prepared using the AlphaScreen Nickel Chelate Acceptor beads (20 μg/mL) and 0.5 mM DTT in assay buffer for 3 h at 4°C. One microliter of the small compound (2 mM) was bound at the bottom of each well in 384-well plates. Then, 10 μL of each solution was mixed in each well and incubated at room temperature for 20 min. Alpha assay measurements were performed at room temperature using the EnSpire plate reader (PerkinElmer, Waltham, MA, USA) with the AlphaScreen protocol. The plate reader excited the donor beads at 660 nm and detected emission signals from acceptor breads at 520–620 nm. The % inhibition was calculated as follows:

$$(\mathrm{LC}–X)/(\mathrm{LC}-\mathrm{HC})\times 100, \quad \text{wherein}$$

LC denotes mean of low control (+*CTBP-AS*, +PSF, and 1% dimethyl sulfoxide (DMSO)); HC denotes mean of high control (+*CTBP1-AS*, −PSF, and 1% DMSO); *X* denotes measured signal in the presence of each compound.

For the analysis of dose–response, alpha assay was performed at seven concentrations (20, 5, 1.25, 0.313, 0.0781, 0.0195, and 0.00488 μg/mL). IC_{50} is estimated by the dose–response curve where % inhibition is 50.

The chemical libraries containing the compounds used for screening were provided by the RIKEN Natural Product Depository (NPDepo: 19,840 compounds), University of Tokyo Core library (9,600 compounds), known drugs (3,865compounds), and the National Institute of Advanced Industrial Science and Technology (AIST) library (22,656 compounds).

2D and 3D structural similarity analysis of small compounds

For the similarity searches, 2D fingerprints [Molecular ACCess System (MACCS), extended connectivity fingerprint 4 (ECFP4), and graph pi-donor-acceptor-polar-hydrophobe fingerprints 4 (GpiDAPH4)] and a 3D shape similarity measure (TanimotoCombo) were employed on Pipeline Pilot 2019 (Dassault Systèmes, San Diego, CA), Molecular Operating Environment (MOE) 2019.0102 (Chemical Computing Group, Montreal, Quebec, Canada), and Rapid Overlay of Chemical Structures (ROCS) 3.2.0.4 (OpenEye Scientific Software, Santa Fe, NM). We obtained the chemicals used in the screening assays from Namiki Shoji (C-65: NS-013291854; N-3: NS-013144661) (Tokyo, Japan).

Statistics and reproducibility

All experiments were performed at least twice, and similar results were obtained. Data are expressed as mean ± SD. Two-sided Student's *t* test was performed to determine the statistical

significance between two groups. When more than two samples were compared, a one-way ANOVA with post hoc Tukey test was performed. Statistical tests are described in the figure legends. Statistical significance was defined as $P < 0.05$. The qPCR analyses of the cell lines were performed in technical replicates. For other analyses, biological replicates were used. MS Excel (Microsoft, Redmond, WA, USA) and GraphPad Prism ver. 6.0 (La Jolla, CA, USA) were used for statistical analyses.

Supplementary material

Supplementary material is available at *PNAS Nexus* online.

Funding

This work was supported by grants from the P-CREATE from the Ministry of Education, Culture, Sports, Science and Technology, Japan (MI.Y. and S.I.); the Japan Society for the Promotion of Science, Japan [number 21H04829 (S.I.) and number 20K07350 (K.T.)]; and the Naito Foundation (K.T.), Takeda Science Foundation (K.T. and S.I.), Japan.

Author contributions

K.T. and S.I. designed the research; K.T. and S.M. performed experiments; S.A. contributed the methods for the alkylation of RNA probes; T.H. performed computer analysis of small molecules; MA.Y. and T.D. produced Flag peptide; K.S., MI.Y., and H.O. provide libraries of small molecules; K.T., T.H., MA.Y., T.D., and S.I. wrote the manuscript; and S.I. supervised the study.

Data availability

All study data are included in the article and/or in the online supplementary material.

References

1 Gerstberger S, Hafner M, Tuschl T. 2014. A census of human RNA-binding proteins. *Nat Rev Genet*. 15:829–845.
2 Dang H, *et al.* 2017. Oncogenic activation of the RNA binding protein NELFE and MYC signaling in hepato-cellular carcinoma. *Cancer Cell* 32:101–114.
3 Conlon EG, Manley JL. 2017. RNA-binding proteins in neurodegeneration: mechanisms in aggregate. *Genes Dev*. 31:1509–1528.
4 Knott GJ, Bond CS, Fox AH. 2016. The DBHS proteins SFPQ, NONO and PSPC1: a multipurpose molecular scaffold. *Nucleic Acids Res*. 44:3989–4004.
5 Patton JG, Porro EB, Galceran J, Tempst P, Nadal-Ginard B. 1993. Cloning and characterization of PSF, a novel pre-mRNA splicing factor. *Genes Dev*. 7:393–406.
6 Lee M, *et al.* 2015. The structure of human SFPQ reveals a coiled-coil mediated polymer essential for functional aggregation in gene regulation. *Nucleic Acids Res*. 43:3826–3840.
7 Takeuchi A, *et al.* 2018. Loss of Sfpq causes long-gene transcriptopathy in the brain. *Cell Rep*. 23:1326–1341.
8 Cosker KE, Fenstermacher SJ, Pazyra-Murphy MF, Elliott HL, Segal RA. 2016. The RNA-binding protein SFPQ orchestrates an RNA regulon to promote axon viability. *Nat Neurosci*. 19:690–696.
9 Takayama K, Fujiwara K, Inoue S. 2019. Amyloid precursor protein, an androgen-regulated gene, is targeted by RNA-binding protein PSF/SFPQ in neuronal cells. *Genes Cells*. 24:719–730.
10 Ray P, *et al.* 2011. PSF suppresses tau exon 10 inclusion by interacting with a stem-loop structure downstream of exon 10. *J Mol Neurosci*. 45:453–466.
11 Takayama K, *et al.* 2013. Androgen-responsive long noncoding RNA CTBP1-AS promotes prostate cancer. *EMBO J*. 32:1665–1680.
12 Mathur M, Tucker PW, Samuels HH. 2001. PSF is a novel corepressor that mediates its effect through Sin3A and the DNA binding domain of nuclear hormone receptors. *Mol Cell Biol*. 21:2298–2311.
13 Takayama K, *et al.* 2017. Dysregulation of spliceosome gene expression in advanced prostate cancer by RNA-binding protein PSF. *Proc Natl Acad Sci U S A*. 114:10461–10466.
14 Ji Q, *et al.* 2014. Long non-coding RNA MALAT1 promotes tumour growth and metastasis in colorectal cancer through binding to SFPQ and releasing oncogene PTBP2 from SFPQ/PTBP2 complex. *Br J Cancer*. 111:736–748.
15 Pellarin I, *et al.* 2020. Splicing factor proline- and glutamine-rich (SFPQ) protein regulates platinum response in ovarian cancer-modulating SRSF2 activity. *Oncogene* 39:4390–4403.
16 Chen CD, *et al.* 2004. Molecular determinants of resistance to antiandrogen therapy. *Nat Med*. 10:33–39.
17 Cai C, *et al.* 2011. Androgen receptor gene expression in prostate cancer is directly suppressed by the androgen receptor through recruitment of lysine-specific demethylase 1. *Cancer Cell* 20:457–471.
18 Chng KR, Cheung E. 2013. Sequencing the transcriptional network of androgen receptor in prostate cancer. *Cancer Lett*. 340:254–260.
19 Gorrini C, *et al.* 2014. Estrogen controls the survival of BRCA1-deficient cells via a PI3K-NRF2-regulated pathway. *Proc Natl Acad Sci U S A*. 111:4472–4477.
20 Musgrove EA, Sutherland RL. 2009. Biological determinants of endocrine resistance in breast cancer. *Nat Rev Cancer*. 9:631–643.
21 Zhao L, Zhou S, Gustafsson JÅ. 2019. Nuclear receptors: recent drug discovery for cancer therapies. *Endocr Rev*. 40:1207–1249.
22 Lupien M, *et al.* 2008. Foxa1 translates epigenetic signatures into enhancer-driven lineage-specific transcription. *Cell* 132:958–970.
23 Mitobe Y, *et al.* 2020. PSF promotes ER-positive breast cancer progression via posttranscriptional regulation of ESR1 and SCFD2. *Cancer Res*. 80:2230–2242.
24 Takayama K, *et al.* 2021. Targeting epigenetic and posttranscriptional gene regulation by PSF impairs hormone therapy-refractory cancer growth. *Cancer Res*. 81:3495–3508.
25 Wang E, *et al.* 2019. Targeting an RNA-binding protein network in acute myeloid leukemia. *Cancer Cell* 35:369–384.e7.
26 Seiler M, *et al.* 2018. H3B-8800, an orally available small-molecule splicing modulator, induces lethality in spliceosome-mutant cancers. *Nat Med*. 24:497–504.
27 Holmes AG, *et al.* 2022. A MYC inhibitor selectively alters the MYC and MAX cistromes and modulates the epigenomic landscape to regulate target gene expression. *Sci Adv*. 8:eabh3635.
28 Wells JA, McClendon CL. 2007. Reaching for high-hanging fruit in drug discovery at protein-protein interfaces. *Nature* 450:1001–1009.
29 Arkin MR, Wells JA. 2004. Small-molecule inhibitors of protein-protein interactions: progressing towards the dream. *Nat Rev Drug Discov*. 3:301–317.
30 Song X, *et al.* 2016. Development of potent small-molecule inhibitors to drug the undruggable steroid receptor coactivator-3. *Proc Natl Acad Sci U S A*. 113:4970–4975.
31 Han H, *et al.* 2019. Small-molecule MYC inhibitors suppress tumor growth and enhance immunotherapy. *Cancer Cell* 36:483–497.e15.

32 Vassilev LT, *et al.* 2004. In vivo activation of the p53 pathway by small-molecule antagonists of MDM2. *Science* 303:844–848.

33 Manzoni L, *et al.* 2018. Interfering with HuR-RNA interaction: design, synthesis and biological characterization of tanshinone mimics as novel, effective HuR inhibitors. *J Med Chem*. 61:1483–1498.

34 Wu X, *et al.* 2015. Identification and validation of novel small molecule disruptors of HuR-mRNA interaction. *ACS Chem Biol*. 10:1476–1484.

35 Kayukawa T, *et al.* 2020. Identification of a juvenile-hormone signaling inhibitor via high-throughput screening of a chemical library. *Sci Rep*. 10:18413 .

36 Hashimoto J, *et al.* 2009. Novel in vitro protein fragment complementation assay applicable to high-throughput screening in a 1536-well format. *J Biomol Screen*. 14:970–979.

37 Miyazaki I, Simizu S, Ichimiya H, Kawatani M, Osada H. 2008. Robust and systematic drug screening method using chemical arrays and the protein library: identification of novel inhibitors of carbonic anhydrase II. *Biosci Biotechnol Biochem*. 72:2739–2749.

38 Kudo N, Ito A, Arata M, Nakata A, Yoshida M. 2018. Identification of a novel small molecule that inhibits deacetylase but not defatty-acylase reaction catalysed by SIRT2. *Philos Trans R Soc Lond B Biol Sci*. 373:20170070.

39 Lipinski CA, Lombardo F, Dominy BW, Feeney PJ. 2001. Experimental and computational approaches to estimate solubility and permeability in drug discovery and development settings. *Adv Drug Deliv Rev*. 46:3–26.

40 Veber DF, *et al.* 2002. Molecular properties that influence the oral bioavailability of drug candidates. *J Med Chem*. 45:2615–2623.

41 Hann MM, Oprea TI. 2004. Pursuing the leadlikeness concept in pharmaceutical research. *Curr Opin Chem Biol*. 8:255–263.

42 Antonarakis ES, *et al.* 2014. AR-V7 and resistance to enzalutamide and abiraterone in prostate cancer. *N Engl J Med*. 371: 1028–1038.

43 Cheng Z, *et al.* 2022. Long noncoding RNA LHFPL3-AS2 suppresses metastasis of non-small cell lung cancer by interacting with SFPQ to regulate TXNIP expression. *Cancer Lett*. 531:1–13.

44 He SW, *et al.* 2020. AR-induced long non-coding RNA LINC01503 facilitates proliferation and metastasis via the SFPQ-FOSL1 axis in nasopharyngeal carcinoma. *Oncogene* 39:5616–5632.

45 Bi O, *et al.* 2021. SFPQ promotes an oncogenic transcriptomic state in melanoma. *Oncogene* 40(33):5192–5203.

46 Adachi S, Natsume T. 2015. Purification of noncoding RNA and bound proteins using FLAG peptide-conjugated antisense-oligonucleotides. *Methods Mol Biol*. 1262:265–274.

47 Cole MA, *et al.* 2009. A chemical approach to immunoprotein engineering: chemoselective functionalization of thioester proteins in their native state. *Chembiochem* 10:1340–1343.